JGR Space Physics

RESEARCH ARTICLE
10.1029/2018JA026374

Cyclotron Acceleration of Relativistic Electrons Through Landau Resonance With Obliquely Propagating Whistler-Mode Chorus Emissions

Yoshiharu Omura[1], Yi-Kai Hsieh[1], John C. Foster[2], Philip J. Erickson[2], Craig A. Kletzing[3], and Daniel N. Baker[4]

[1]Research Institute for Sustainable Humanosphere, Kyoto University, Kyoto, Japan, [2]Haystack Observatory, Massachusetts Institute of Technology, Westford, MA, USA, [3]Department of Physics and Astronomy, University of Iowa, Iowa City, IA, USA, [4]Laboratory for Atmospheric and Space Physics, University of Colorado Boulder, Boulder, CO, USA

Key Points:
- Oblique chorus waves can accelerate relativistic electrons effectively through Landau resonance
- The acceleration is due to the perpendicular component of the wave electric field
- Nonlinear trapping conditions and efficiency of electron acceleration are confirmed by spacecraft observation

Correspondence to:
Y. Omura,
omura@rish.kyoto-u.ac.jp

Citation:
Omura, Y., Hsieh, Y.-K., Foster, J. C., Erickson, P. J., Kletzing, C. A., & Baker, D. N. (2019). Cyclotron acceleration of relativistic electrons through Landau resonance with obliquely propagating whistler-mode chorus emissions. *Journal of Geophysical Research: Space Physics*, *124*, 2795–2810. https://doi.org/10.1029/2018JA026374

Received 6 DEC 2018
Accepted 5 APR 2019
Accepted article online 12 APR 2019
Published online 24 APR 2019

Abstract Efficient acceleration of relativistic electrons at Landau resonance with obliquely propagating whistler-mode chorus emissions is confirmed by theory, simulation, and observation. The acceleration is due to the perpendicular component of the wave electric field. We first review theoretical analysis of nonlinear motion of resonant electrons interacting with obliquely propagating whistler-mode chorus. We have derived formulae of inhomogeneity factors for Landau and cyclotron resonances to analyze nonlinear wave trapping of energetic electrons by an obliquely propagating chorus element. We performed test particle simulations to confirm that nonlinear wave trapping by both Landau and cyclotron resonances can take place for a wide range of energies. For an element of large amplitude chorus waves observed by the Van Allen Probes, we have performed detailed analyses of the wave form data based on theoretical framework of nonlinear trapping of resonant electrons. We compare the efficiencies of accelerations by cyclotron and Landau resonances. We find significant acceleration can take place both in Landau and cyclotron resonances. What controls the dynamics of relativistic electrons in the Landau resonance is the perpendicular field components rather than the parallel electric field of the oblique chorus wave. In evaluating the efficiency of nonlinear trapping, we have taken into account variation of the wave trapping potential structure controlled by the inhomogeneity factors.

1. Introduction

Whistler-mode chorus emissions are frequently observed in the inner magnetosphere, being generated by energetic electrons injected from the magnetotail at the time of the geomagnetic field disturbances such as substorms and magnetic storms, as demonstrated by recent statistical studies based on observation by Time History of Events and Macroscale Interactions during Substorms (THEMIS) probes and Van Allen Probes (Li et al., 2009, 2011, 2016). A typical chorus emission is a coherent wave with rising-tone frequency. The initial part of the emissions at the lower frequency is due to the linear instability driven by a temperature anisotropy which develops through injection of energetic electrons into the inner magnetosphere. A whistler-mode wave with the maximum linear growth rate grows at a wave normal angle parallel to the background magnetic field. Once the growing wave amplitude attains a threshold amplitude, the wave packet grows through the nonlinear wave growth process associated with formation of an electromagnetic electron hole in the velocity phase space (Omura et al., 2008, 2012). The wave packet grows due to the frequency increase induced by the electron hole. Once the wave amplitude exceeds the optimum wave amplitude (Omura & Nunn, 2011), the wave growth saturates, and the amplitude decreases gradually. New seed waves, which can trigger the nonlinear wave growth process, are generated slightly upstream from the equator because of the phase-modulated resonant electrons moving in the opposite direction from the downstream to the upstream of the wave propagation. The phases of the resonant electrons are modulated with the frequency of the foregoing saturated wave packet, which is higher than that of the original triggering wave. The phase-modulated electrons generate a new triggering wave with faster oscillations matching the foregoing wave packet. When this growth process is repeated many times, many new subpackets are formed at progressively higher frequencies as time proceeds (Shoji & Omura, 2013).

The process of the subpacket formation with increasing frequencies continues until the threshold amplitude exceeds the optimum amplitude or until the cyclotron damping near the electron cyclotron frequency becomes dominant suppressing the generation of seed waves as triggering waves. Starting from the low frequency 0.2 f_{cEQ}, where f_{cEQ} is the electron cyclotron frequency at the equator, a chorus element can reach a high frequency 0.8 f_{cEQ}, as observed by THEMIS near the magnetic equator (Kurita et al., 2012). Electromagnetic particle simulations with assumption of purely parallel propagation of whistler-mode waves also show formation of chorus elements from 0.1–0.2 f_{cEQ} to 0.7–0.8 f_{cEQ} (Hikishima et al., 2009; Katoh & Omura, 2007).

Propagating away from the equator, a chorus element undergoes efficient wave growth due to the increasing gradient of the ambient magnetic field (Omura et al., 2009). Because the wave normal angle deviates from the parallel direction through propagation in the dipole magnetic field, nonlinear damping occurs near half the electron cyclotron frequency, separating the chorus element into a lower band and a upper band at 0.5 f_{cEQ} (Habagishi et al., 2014; Hsieh & Omura, 2018; Yagitani et al., 2014). Since propagation characteristics of the upper-band chorus and the lower-band chorus are different (Bell et al., 2009), spacecraft may also observe lower-band and upper-band chorus emissions from different sources and of different properties concurrently (Li et al., 2016). Obliquely propagating chorus waves with large amplitudes cause induced nonlinear scattering that keeps the wave normal angles small (Ganguli et al., 2012). It is important to understand resonant electron acceleration and associated wave damping at oblique wave normal angles (Artemyev et al., 2013, 2016; Shklyar & Matsumoto, 2009).

A recent analysis of wave and particle data obtained by the Van Allen Probes (Foster et al., 2017) demonstrates highly efficient acceleration of radiation belt electrons by whistler-mode chorus emissions. The analysis has confirmed that the acceleration is mostly due to the cyclotron resonance of relativistic electrons with chorus emissions propagating quasi-parallel to the ambient magnetic field. As the energy of an electron becomes relativistic (1–2 MeV), the parallel resonance velocity approaches to zero near the equator, where nonlinear trapping of resonant electrons becomes possible, resulting in relativistic turning acceleration (Omura et al., 2007) and ultra relativistic acceleration (Summers & Omura, 2007). The detailed subpacket analysis shows that there arises a parallel wave electric field that can trap energetic electrons through Landau resonance, but the acceleration by the parallel wave electric field is effective for energies below 1 MeV (Foster et al., 2017). A recent test particle simulation (Hsieh & Omura, 2017a), however, shows that the perpendicular wave electric field can also play a significant role in trapping and accelerating relativistic electrons through Landau resonance.

We present a theoretical analysis of Landau resonance acceleration and verify it by a test particle simulation and by analysis of chorus emissions observed by Van Allen Probes. We compare the efficiencies of accelerations by cyclotron and Landau resonances. The efficiency of acceleration depends on the nonlinear motion of resonant electrons trapped in the wave potentials. The nonlinear dynamics of resonant electrons are controlled by the inhomogeneity factors S_0 and S_1 for Landau and cyclotron resonances. We for the first time have obtained formulae of the inhomogeneity factors for evaluation at fixed positions along the magnetic field line in sections 3 and 5, while Nunn and Omura (2015) derived the formula for evaluation as observed from a moving resonant electron, which could not be applied to spacecraft observations. Section 4 gives a simple explanation of Landau resonant cyclotron acceleration. The formulae of the inhomogeneity factors are checked with the test particle simulation in section 6. Applying the formulae to a chorus emission observed by Van Allen Probes, we evaluate acceleration efficiencies by Landau and cyclotron resonances and discuss the overall acceleration efficiency by chorus emissions in section 7. Section 8 gives summary and discussion.

2. Circularly Polarized Wave Fields

We assume a whistler-mode wave with a frequency ω propagating in a (x, z) plane with a wave normal vector k at propagation angle θ with respect to the background magnetic field B_0 taken along the z axis as shown in Figure 1a. We have

$$k_z = k\cos\theta, \qquad k_x = k\sin\theta, \qquad k_y = 0, \tag{1}$$

where k and ω are given by the cold plasma dispersion relation, that is, the Appleton-Hartree equation (Stix, 1992). Defining the amplitudes of the wave electric and magnetic field oscillations in the (x, y, z) directions

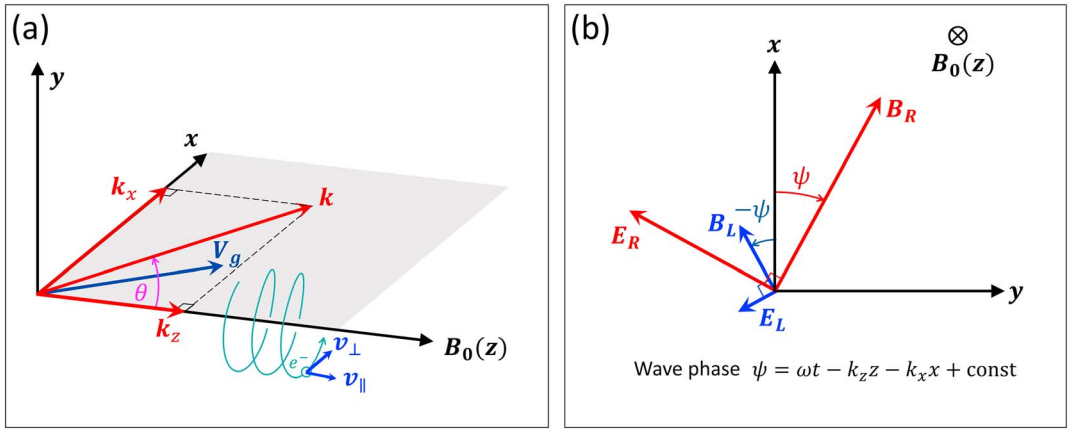

Figure 1. (a) Configuration of wave vectors, electron velocities, background magnetic field, and coordinates. (b) Decomposition of the perpendicular wave electric and magnetic fields into R mode (red) and L mode (blue).

as E_x^w, E_y^w, E_z^w, B_x^w, B_y^w, B_z^w, we can express the wave fields by the following equations.

$$\boldsymbol{E}_w = \boldsymbol{e_x} E_x^w \sin\psi - \boldsymbol{e_y} E_y^w \cos\psi + \boldsymbol{e_z} E_z^w \sin\psi, \tag{2}$$

$$\boldsymbol{B}_w = \boldsymbol{e_x} B_x^w \cos\psi + \boldsymbol{e_y} B_y^w \sin\psi - \boldsymbol{e_z} B_z^w \cos\psi, \tag{3}$$

where e_x, e_y, and e_z are unit vectors in the x, y, and z directions, and the quantities with superscript w are positive wave amplitudes. The detailed expressions of the wave amplitudes are given in Hsieh and Omura (2017a). The wave phase ψ is defined by

$$\psi = \omega t - k_x x - k_z z + \text{const}. \tag{4}$$

As illustrated in Figure 1b, the wave fields B_x, B_y, E_x, and E_y perpendicular to the static magnetic field B_0 are decomposed into a right-hand circularly polarized wave (R mode)

$$\boldsymbol{E}_\mathrm{R} = E_\mathrm{R}^w[\boldsymbol{e_x}\sin\psi - \boldsymbol{e_y}\cos\psi], \tag{5}$$

$$\boldsymbol{B}_\mathrm{R} = B_\mathrm{R}^w[\boldsymbol{e_x}\cos\psi + \boldsymbol{e_y}\sin\psi], \tag{6}$$

and a left-handed circularly polarized wave (L mode)

$$\boldsymbol{E}_\mathrm{L} = E_\mathrm{L}^w[\boldsymbol{e_x}\sin(-\psi) - \boldsymbol{e_y}\cos(-\psi)], \tag{7}$$

$$\boldsymbol{B}_\mathrm{L} = B_\mathrm{L}^w[\boldsymbol{e_x}\cos(-\psi) + \boldsymbol{e_y}\sin(-\psi)], \tag{8}$$

where

$$E_\mathrm{R}^w = \frac{E_x^w + E_y^w}{2};\ E_\mathrm{L}^w = \frac{E_y^w - E_x^w}{2}, \tag{9}$$

and

$$B_\mathrm{R}^w = \frac{B_x^w + B_y^w}{2};\ B_\mathrm{L}^w = \frac{B_x^w - B_y^w}{2}. \tag{10}$$

Both wave amplitudes E_L^w and B_L^w of the L mode can be negative or positive, while the wave amplitude E_R^w and B_R^w of the R mode are defined as positive values. In either case, Poynting vectors of R and L modes are in the positive z direction along the magnetic field line. We define the ratios of the electric and magnetic wave fields

$$U_\mathrm{R} = E_\mathrm{R}^w/B_\mathrm{R}^w;\ U_\mathrm{L} = E_\mathrm{L}^w/B_\mathrm{L}^w. \tag{11}$$

We also have the wave fields E_z^w and B_z^w parallel to the static magnetic field. From the Maxwell's equations, we have

$$\boldsymbol{k} \times \boldsymbol{E} = \omega \boldsymbol{B}. \tag{12}$$

Solving for E_z^w and B_z^w, we obtain

$$E_z^w = \frac{k_z}{k_x}[(U_R - V_{p\parallel})B_R^w - (U_L - V_{p\parallel})B_L^w], \tag{13}$$

$$B_z^w = \frac{k_x}{\omega}(U_R B_R^w + U_L B_L^w), \tag{14}$$

where $V_{p\parallel}$ is the parallel phase velocity given by ω/k_z.

3. Dynamics of Landau Resonant Electrons

From the relativistic equations of motion for circularly polarized waves (Omura, Zhao, et al., 2012) and adding effects of the parallel wave fields E_z^w and B_z^w, we obtain the following equations.

$$\frac{\mathrm{d}(\gamma v_\parallel)}{\mathrm{d}t} = \frac{e}{m_0}\left[v_\perp B_R^w \sin(\phi - \psi) + v_\perp B_L^w \sin(\phi + \psi) - E_z^w \sin\psi\right] - \frac{\gamma v_\perp^2}{2B_0}\frac{\mathrm{d}B_0}{\mathrm{d}z}, \tag{15}$$

$$\frac{\mathrm{d}(\gamma v_\perp)}{\mathrm{d}t} = \frac{e}{m_0}\left[(U_R - v_\parallel)B_R^w \sin(\phi - \psi) + (U_L - v_\parallel)B_L^w \sin(\phi + \psi)\right] + \frac{\gamma v_\perp v_\parallel}{2B_0}\frac{\mathrm{d}B_0}{\mathrm{d}z}, \tag{16}$$

$$\frac{\mathrm{d}\phi}{\mathrm{d}t} = \frac{e}{\gamma m_0}\left[\frac{U_R - v_\parallel}{v_\perp}B_R^w \cos(\phi - \psi) + \frac{U_L - v_\parallel}{v_\perp}B_L^w \cos(\phi + \psi) - B_z^w \cos\psi + B_0\right], \tag{17}$$

where ϕ is a gyrophase of an electron, and ψ is a phase of a wave magnetic field. We assume an electron moving along the ambient magnetic field along the z axis, and the center of cyclotron motion is at $x = 0$. The wave phase observed by the gyrating electron is given by

$$\psi = \omega t - k_z z - k_x \rho \sin\phi + \mathrm{const} = \psi_B - \beta \sin\phi, \tag{18}$$

where ψ_B ($= \omega t - k_z z +$ const) is a wave phase at the gyro-center, ρ is the cyclotron radius given by $\rho = \gamma v_\perp/\Omega_e$, and

$$\beta = \frac{\gamma v_\perp k_x}{\Omega_e}. \tag{19}$$

The wave phase at the gyro-center is modulated by the cyclotron motion because of the perpendicular wave number k_x. The wave field with the modulated phase can be expanded into a series of Bessel functions as given by

$$\sin(\phi - \psi) = \sum_{n=-\infty}^{\infty} J_{n-1}(\beta)\sin\zeta_n, \tag{20}$$

$$\sin(\phi + \psi) = -\sum_{n=-\infty}^{\infty} J_{n+1}(\beta)\sin\zeta_n, \tag{21}$$

$$\sin(\psi) = -\sum_{n=-\infty}^{\infty} J_n(\beta)\sin\zeta_n, \tag{22}$$

where $\zeta_n = n\phi - \psi_B$. We now assume a particle undergoing Landau resonance ($n = 0$), and its motion is mostly described by

$$\frac{\mathrm{d}(\gamma v_\parallel)}{\mathrm{d}t} = \frac{e}{m_0}\left[v_\perp B_R^w J_{-1}(\beta) - v_\perp B_L^w J_1(\beta) + E_z^w J_0(\beta)\right]\sin\zeta_0 - \frac{\gamma v_\perp^2}{2B_0}\frac{\mathrm{d}B_0}{\mathrm{d}z}, \tag{23}$$

$$\frac{\mathrm{d}(\gamma v_\perp)}{\mathrm{d}t} = \frac{e}{m_0}\left[(U_R - v_\parallel)B_R^w J_{-1}(\beta) - (U_L - v_\parallel)B_L^w J_1(\beta)\right]\sin\zeta_0 + \frac{\gamma v_\perp v_\parallel}{2B_0}\frac{\mathrm{d}B_0}{\mathrm{d}z}, \tag{24}$$

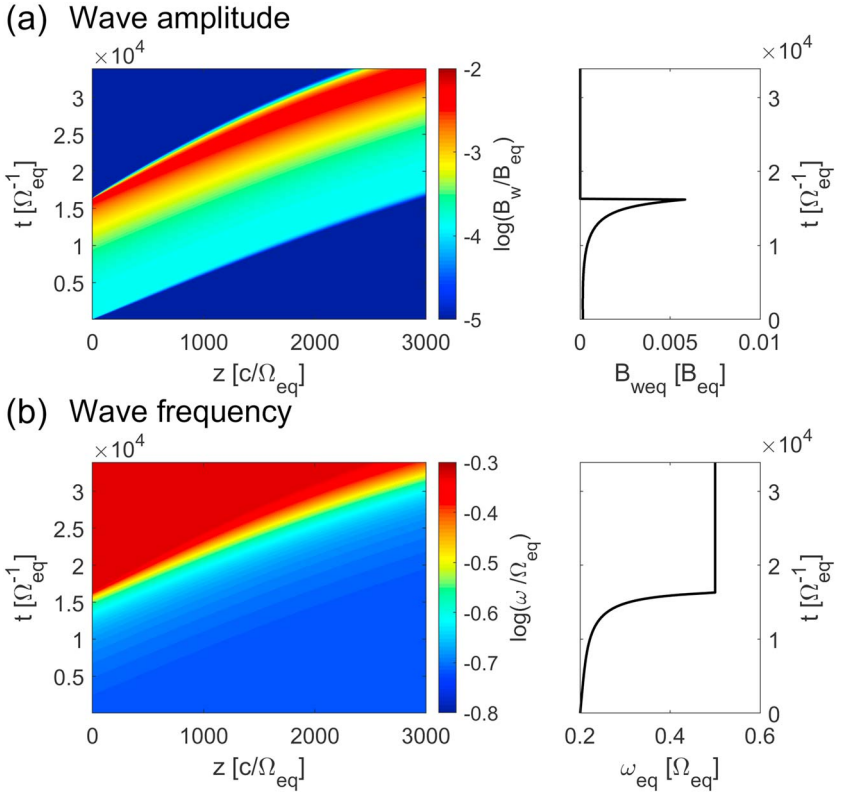

Figure 2. The oblique whistler-mode wave model with wave normal angle 10° assumed in the test particle simulations. (a) Spatial and temporal evolution of the wave amplitude (left).Wave amplitude at the equator (right). (b) Spatial and temporal evolution of the wave frequency (left). Wave frequency at the equator (right).

$$\frac{d\zeta_0}{dt} = k_z v_{\parallel} - \omega, \tag{25}$$

where we have neglected the wave effect on the gyrophase variation, assuming $B_R^w, B_L^w, B_z^w \ll B_0$.

The kinetic energy is given by

$$K = m_0 c^2(\gamma - 1). \tag{26}$$

Since an obliquely propagating wave is decomposed into three components, that is, parallel component, perpendicular component with right-handed circular polarization, and perpendicular component with left-handed circular polarization, we have three terms of particle accelerations as in

$$\frac{dK}{dt} = e\sum_{n=-\infty}^{\infty}\left[v_{\parallel}E_z^w J_n(\beta) + v_{\perp}E_R^w J_{n-1}(\beta) - v_{\perp}E_L^w J_{n+1}(\beta)\right]\sin\zeta_n. \tag{27}$$

The variation of the kinetic energy K of an electron trapped by a wave potential due to Landau resonance ($n = 0$) is given by

$$\frac{dK_0}{dt} = e\left[V_{p\parallel}E_z^w J_0(\beta) - v_{\perp}E_y^w J_1(\beta)\right]\sin\zeta_0, \tag{28}$$

where the resonance velocity V_R is given by the parallel phase velocity $V_{p\parallel} = \omega/k_z$, and the perpendicular velocity is calculated by

$$v_{\perp} = \sqrt{c^2(1-\gamma^{-2}) - V_{p\parallel}^2}. \tag{29}$$

We integrate the energy variation over half a wave period δt and sum them over a duration of a subpacket as

$$\Delta K_0 = \sum_{\delta t}\frac{dK_0}{dt}\cdot\frac{V_{g\parallel}\delta t}{V_{g\parallel} - V_{p\parallel}}\left(1 - \frac{V_{g\parallel}V_{p\parallel}}{c^2}\right). \tag{30}$$

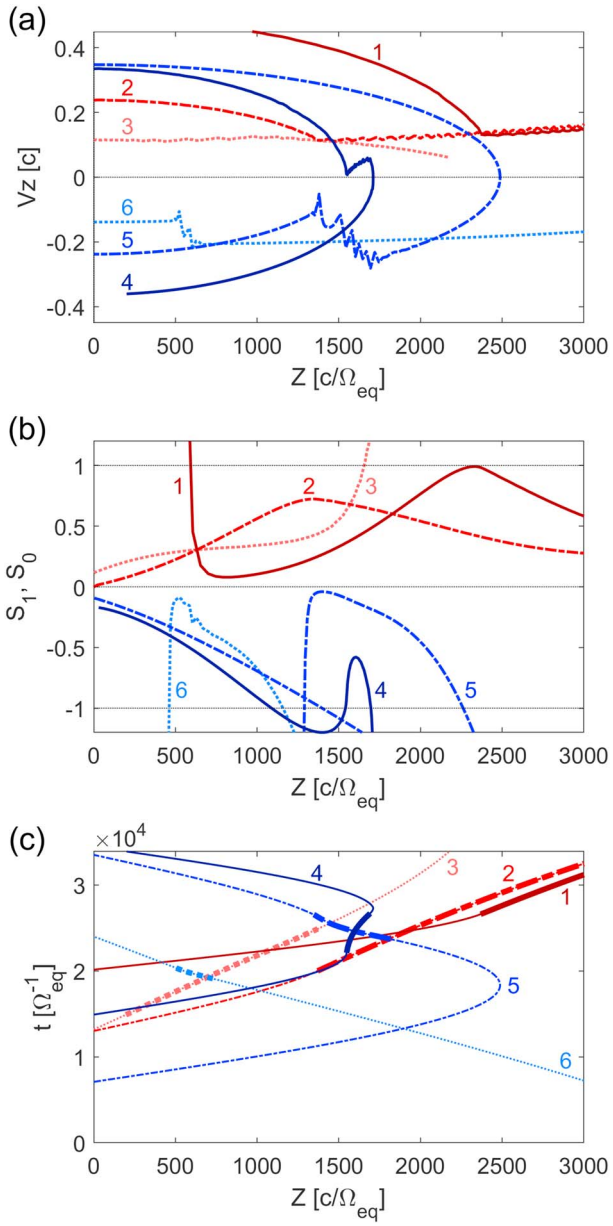

Figure 3. Examples of electrons undergoing nonlinear trapping by the oblique whistler-mode wave. Trajectories in shades of red (lines 1–3) are for electrons undergoing Landau resonance, and ones in shades of blue (lines 4–6) are for electron undergoing cyclotron resonance. The solid, dash-dotted, and dotted lines denote electrons with energy 2, 0.2, and 0.02 MeV, respectively. (a) Trajectories in $z - v_\parallel$ phase space. (b) Trajectories in position and Inhomogeneity factor S_0 or S_1. (c) Trajectories in position and time. The thicker part of each curve points out the duration when the electron undergoes nonlinear trapping.

From (42) and (44) of Nunn and Omura (2015), we have

$$\frac{\mathrm{d}K_0}{\mathrm{d}t} = \frac{m_0}{k_z}(v_\parallel \omega_{t,0}^2 + v_\perp \omega_{s,0}^2)\sin\zeta_0, \tag{31}$$

where

$$\omega_{t,0}^2 = \frac{ek_z}{m_0}\left[E_z^w J_0(\beta) + v_\perp B_\mathrm{R}^w J_{-1}(\beta) - v_\perp B_\mathrm{L}^w J_1(\beta)\right], \tag{32}$$

$$\omega_{s,0}^2 = \frac{ek_z}{m_0}\left[(U_\mathrm{R} - v_\parallel) B_\mathrm{R}^w J_{-1}(\beta) - (U_\mathrm{L} - v_\parallel) B_\mathrm{L}^w J_1(\beta)\right]. \tag{33}$$

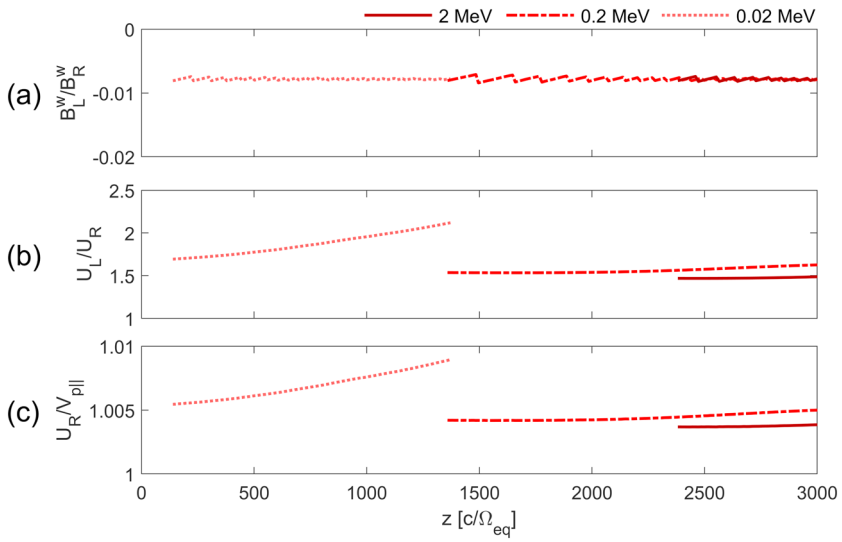

Figure 4. Ratios of wave field components seen by electrons undergoing Landau resonance as functions of z. (a) B_L^w/B_R^w, (b) U_L/U_R, and (c) $U_R/V_{p\|}$.The electrons are the same as the ones shown in Figure 2 in shade of red. The solid, dash-dotted, and dotted lines denote electrons with energy 2, 0.2, and 0.02 MeV, respectively.

Since the whistler-mode waves are mostly right-handed, we have $B_L^w \ll B_R^w$. We checked the values of U_R and U_L in a test particle simulation of an obliquely propagating chorus emission as shown in Figure 2. Typical trajectories of resonant electrons with kinetic energies 0.02, 0.2, and 2 MeV are plotted in Figure 3. The Landau resonant electrons are plotted in red. The ratios of B_L^w/B_R^w, U_L/U_R, and $U_R/V_{p\|}$ as observed by these trapped resonant electrons are plotted as functions of z in Figure 4. We find that $U_R \sim V_{p\|}$ and $B_L^w/B_R^w \ll 1$, and we can assume $\omega_{s,0}^2 \sim 0$ for Landau resonance.

$$\frac{dK_0}{dt} \sim \frac{m_0}{k_z} v_\| \omega_{t,0}^2 \sin\zeta_0. \tag{34}$$

The averaged phase angle ζ_0 is given by the second-order resonance condition

$$\frac{d^2\zeta_0}{dt^2} = \omega_{t1,0}^2 \left(\sin\zeta_0 + S_0\right) = 0, \tag{35}$$

where

$$\omega_{t1,0}^2 = \frac{\omega_{t,0}^2}{\gamma}\left(1 - \frac{v_\|^2}{c^2}\right), \tag{36}$$

and

$$S_0 = -\frac{k_z}{\omega_{t1,0}^2}\left(\frac{dV_{p\|}}{dt} + \frac{v_\perp^2}{2\Omega_e}\frac{d\Omega_e}{dz}\right). \tag{37}$$

When $|S_0| < 1$, (35) is satisfied, and nonlinear trapping of resonant electrons becomes possible. The time derivative of $V_{p\|}$ as observed by an electron can be rewritten as

$$\frac{dV_{p\|}}{dt} = \frac{1}{k_z}\frac{d\omega}{dt} - \frac{\omega}{k_z^2}\frac{dk_z}{dt}. \tag{38}$$

Assuming that ω is uniform in the perpendicular direction x, we have

$$\frac{d\omega}{dt} = \left(1 - \frac{v_\|}{V_{g\|}}\right)\frac{\partial\omega}{\partial t}. \tag{39}$$

It is difficult to evaluate the spatial variation of the wave number k_z determined by the exact oblique dispersion relation. For the wave normal angles satisfying the quasi-parallel condition $\sin^2\theta << 1$, we can

approximate the dispersion relation by that of the parallel propagation. From (12) of Omura et al. (2008), we have

$$\frac{\partial k_z}{\partial z} = -\frac{1}{V_{g\parallel}}\frac{\partial k}{\partial t} - \frac{\chi\omega}{2c\xi(\Omega_e-\omega)}\frac{\partial \Omega_e}{\partial z}, \tag{40}$$

where χ and ξ are defined by

$$\chi^2 = 1 - \left(\frac{\omega}{ck}\right)^2 \simeq 1 - \frac{1}{c^2}V_{p\parallel}^2, \tag{41}$$

and

$$\xi^2 = \frac{\omega(\Omega_e-\omega)}{\omega_{pe}^2}. \tag{42}$$

The time derivative of k_z as observed by a resonant electron with $v_\parallel$ is given by

$$\frac{\mathrm{d}k_z}{\mathrm{d}t} = \frac{\partial k_z}{\partial t} + v_\parallel\frac{\partial k_z}{\partial z} = \left(1 - \frac{v_\parallel}{V_{g\parallel}}\right)\frac{\partial k_z}{\partial t} - \frac{\chi\omega v_\parallel}{2c\xi(\Omega_e-\omega)}\frac{\partial \Omega_e}{\partial z}, \tag{43}$$

where we use the wave phase relation $\partial k_z/\partial t = -\partial\omega/\partial z$. Substituting (39) and (43) into (38) and using the Landau resonance condition $v_\parallel = V_{p\parallel}$, we obtain

$$\frac{\mathrm{d}V_{p\parallel}}{\mathrm{d}t} = \frac{1}{k_z}\left(1 - \frac{V_{p\parallel}}{V_{g\parallel}}\right)^2\frac{\partial\omega}{\partial t} + \frac{\chi V_{p\parallel}^3}{2c\xi(\Omega_e-\omega)}\frac{\partial\Omega_e}{\partial z}. \tag{44}$$

Using (44), we rewrite (37) as

$$S_0 = -\frac{1}{\omega_{t1,0}^2}\left\{\left(1 - \frac{V_{p\parallel}}{V_{g\parallel}}\right)^2\frac{\partial\omega}{\partial t} + \frac{c}{2}\left[\frac{\omega\chi V_{p\parallel}^2}{\xi(\Omega_e-\omega)c^2} + \frac{\omega v_\perp^2}{\Omega_e c V_{p\parallel}}\right]\frac{\partial\Omega_e}{\partial z}\right\}. \tag{45}$$

Substituting $\sin\zeta_0 = -S_0$ into (34), we obtain

$$\frac{\mathrm{d}K_0}{\mathrm{d}t} \sim \frac{\gamma m_0 V_{p\parallel}}{k_z}\left(1 - \frac{V_{p\parallel}^2}{c^2}\right)^{-1}\left\{\left(1 - \frac{V_{p\parallel}}{V_{g\parallel}}\right)^2\frac{\partial\omega}{\partial t} + +\frac{c}{2}\left[\frac{\omega\chi V_{p\parallel}^2}{\xi(\Omega_e-\omega)c^2} + \frac{\omega v_\perp^2}{\Omega_e c V_{p\parallel}}\right]\frac{\partial\Omega_e}{\partial z}\right\}. \tag{46}$$

Equation (46) is valid as far as the electrons are trapped by the nonlinear wave potential moving with $V_{p\parallel}$, namely, $|S_0| < 1$. When a particle is moving away from the equator ($v_\parallel > 0$) in the same direction of a chorus wave, the first term in the brackets is positive because of the rising-tone frequency, and the second term is also positive because of the positive gradient of the magnetic field. Therefore, the kinetic energy of an electron trapped in the nonlinear wave potential always increases.

4. Simple Explanation of Landau Resonant Cyclotron Acceleration

We assume a frame of reference moving with the phase velocity of the wave. We also assume a plane transverse to the phase velocity. The gyro-center of a Landau resonant electron ($v_\parallel = V_{p\parallel}$) remains in this plane. All electromagnetic fields in this plane are stationary. Since the electron undergoes cyclotron motion around the magnetic field aligned oblique to the phase velocity with a wave normal angle θ, the cyclotron motion induces a phase shift by $k_x\rho\sin(\Omega_e t/\gamma)$ in the electromagnetic fields seen by the electron. When the wave phase is modulated with $\sin(\Omega_e t/\gamma)$, each of the electromagnetic field is expanded into a series of Bessel functions with phase variations of $n\Omega_e t/\gamma$. The velocity vector $v_\parallel$ of the resonant electron sees a stationary parallel electric field $E_z^w J_0(\beta)$, while the perpendicular velocity vector $v_\perp$ undergoes cyclotron motion in the right-hand direction with the angular frequency Ω_e/γ. The wave fields observed by the electron contains field components $E_R^w J_1(\beta)$ and $B_R^w J_1(\beta)$, which rotate in the right-hand direction with the cyclotron frequency, and they can be in resonance with the electron undergoing the cyclotron motion, resulting in effective electron acceleration and pitch angle scattering. We call this acceleration as "cyclotron acceleration" through Landau resonance. In addition to the parallel electric field, the electron sees a nonlinear Lorentz force $v_\perp B_R^w J_1(\beta)$ along the magnetic field, which contributes to the nonlinear trapping of resonant electrons.

5. Dynamics of Cyclotron Resonant Electrons

From Nunn and Omura (2015), the time variation of the kinetic energy of a trapped resonant electron due to the $n = 1$ cyclotron resonance is given by

$$\frac{dK_1}{dt} = e\left[v_{\parallel}E_z^w J_1(\beta) + v_{\perp}E_R^w J_0(\beta) - v_{\perp}E_L^w J_2(\beta)\right]\sin\zeta_1, \tag{47}$$

where ζ_1 satisfies the second-order cyclotron resonance condition given by

$$\frac{d^2\zeta_1}{dt^2} = k_z\left(\frac{dv_{\parallel}}{dt} - \frac{dV_R}{dt}\right) = 0, \tag{48}$$

where

$$V_R = \frac{1}{k_z}\left(\omega - \frac{\Omega_e}{\gamma}\right) = V_{p\parallel}\left(1 - \frac{\Omega_e}{\gamma\omega}\right). \tag{49}$$

From (51) of Nunn and Omura (2015), we have

$$\frac{dv_{\parallel}}{dt} = \frac{\omega_{t0,1}^2}{\gamma k_z}\sin\zeta_1 - \frac{v_{\perp}^2}{2\Omega_e}\frac{d\Omega_e}{dz}. \tag{50}$$

We calculate the time derivative of V_R as observed by the cyclotron resonant electron.

$$\frac{dV_R}{dt} = \frac{1}{k_z}\left[\frac{d\omega}{dt} - \frac{v_{\parallel}}{\gamma}\frac{\partial\Omega_e}{\partial z} + \frac{\Omega_e}{\gamma^2}\frac{d\gamma}{dt}\right] - \frac{1}{k_z^2}\left(\omega - \frac{\Omega_e}{\gamma}\right)\frac{dk_z}{dt}. \tag{51}$$

Defining the particle acceleration W_1 as in Nunn and Omura (2015), we have

$$\frac{d\gamma}{dt} = \frac{W_1}{c^2}\sin\zeta, \tag{52}$$

where

$$W_1 = \frac{e}{m_0}\left[v_{\parallel}E_z^w J_1(\beta) + v_{\perp}E_R J_0(\beta) - v_{\perp}E_L J_2(\beta)\right]. \tag{53}$$

Substituting (39), (43), and (52) into (51) and using the first-order resonance condition $v_{\parallel} = V_R$, we obtain

$$\frac{dV_R}{dt} = \frac{\Omega_e W_1}{k_z\gamma^2 c^2}\sin\zeta + \frac{1}{k_z}\left(1 - \frac{V_R}{V_{g\parallel}}\right)^2\frac{\partial\omega}{\partial t} - \frac{V_R}{k_z\gamma}\left[1 + \frac{\chi^2(\Omega - \gamma\omega)}{2(\omega_e - \omega)}\right]\frac{\partial\Omega_e}{\partial z}. \tag{54}$$

Substituting (50) and (54) into (48), we derive the second-order cyclotron resonance condition as

$$\frac{d^2\zeta_1}{dt^2} = \omega_{t1,1}^2(\sin\zeta_1 + S_1) = 0, \tag{55}$$

where

$$\omega_{t1,1}^2 = \frac{1}{\gamma}\left(\omega_{t,1}^2 - \frac{\omega W_1}{c^2}\right), \tag{56}$$

$$S_1 = -\frac{1}{\omega_{t1,1}^2}\left\{\left(1 - \frac{V_R}{V_{g\parallel}}\right)^2\frac{\partial\omega}{\partial t} + \left[\frac{\omega v_{\perp}^2}{2\Omega_e V_{p\parallel}} - \frac{V_R}{\gamma}\left(1 + \frac{\chi^2(\Omega_e - \gamma\omega)}{2(\Omega_e - \omega)}\right)\right]\frac{\partial\Omega_e}{\partial z}\right\}, \tag{57}$$

and

$$\omega_{t,1}^2 = \frac{e}{m_0}k_z\left[E_z^w J_1(\beta) + B_R^w v_{\perp}J_0(\beta) - B_L^w v_{\perp}J_2(\beta)\right]. \tag{58}$$

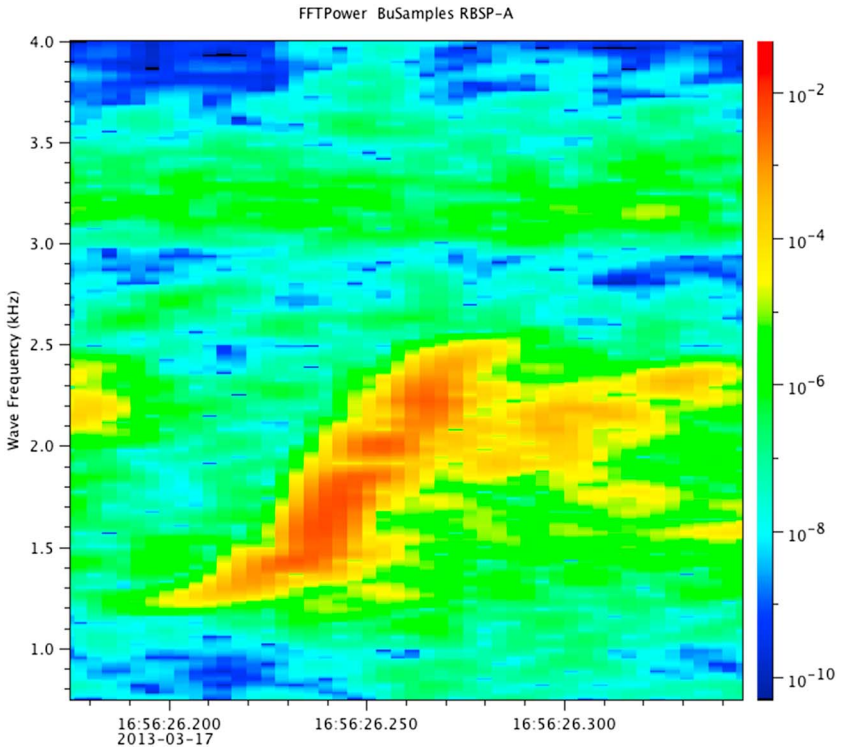

Figure 5. Dynamic spectrum of a chorus element observed by RBSP-A at 16:56:26 on 17 March 2013. Wave properties of the time period between the white dashed lines are further analyzed in Figures 6–9. RBSP = Radiation Belt Storm Probes.

6. Evaluation of Electron Acceleration by Test Particle Simulations

We perform test particle simulations of energetic electrons interacting with a chorus wave packet generated at the equator with a growing amplitude and a rising-tone frequency as shown in the right panels of Figure 2. The variation of the amplitude and frequency is a solution of chorus equations (Omura et al., 2009), which are derived from the nonlinear wave growth theory of chorus emissions. However, we do not intend to discuss the generation process in this section. The purpose of the simulation is to check the nonlinear trapping motion of resonant electrons along with the variation of the inhomogeneity factors S_0 and S_1 obtained in the previous sections. The wave packets propagate away from the equator along the magnetic field in the direction of the static magnetic field with a fixed wave normal angle of 10°. For simplicity, we assume a simplified profile of a chorus element without subpacket structures. We plot trajectories of six electrons in the $z - V_z$, $z - S_{0,1}$, and $z - t$ plains in Figures 3a–3c, respectively. The trajectories in red (particles 1–3) undergo Landau resonance, and those in blue (particles 4–6) undergo $n = 1$ cyclotron resonance. The solid, dash-dot, and dotted lines represent trajectories of particles with different initial kinetic energies 2 MeV, 200 keV, and 20 keV, respectively.

Particles 1–3 all move away from the equator and trapped by the wave packet moving in the same direction. The trajectories 1–3 show oscillations in the parallel velocity V_z indicating nonlinear trapping by the wave packet. During the nonlinear trapping, the inhomogeneity factor S_0 takes the values between 0 and 1 in agreement with the second-order resonance condition for Landau resonance as shown in Figure 3b.

Particles 5 and 6 with energies 0.2 and 0.02 MeV interact with the wave packet through cyclotron resonance, are trapped by it, and move in the opposite direction to its propagation as shown in Figure 3c. The thicker parts of the trajectories in Figure 3c indicate the periods of nonlinear wave trapping. Particle 4 at 2 MeV, on the other hand, get into the cyclotron resonance moving in the same direction with the wave because the cyclotron resonance velocity with $n = 1$ becomes positive because of the high value of the Lorentz factor γ. The inhomogeneity factors S_1 are between −1 and 0 when these particles are trapped by the wave due to $n = 1$ cyclotron resonance.

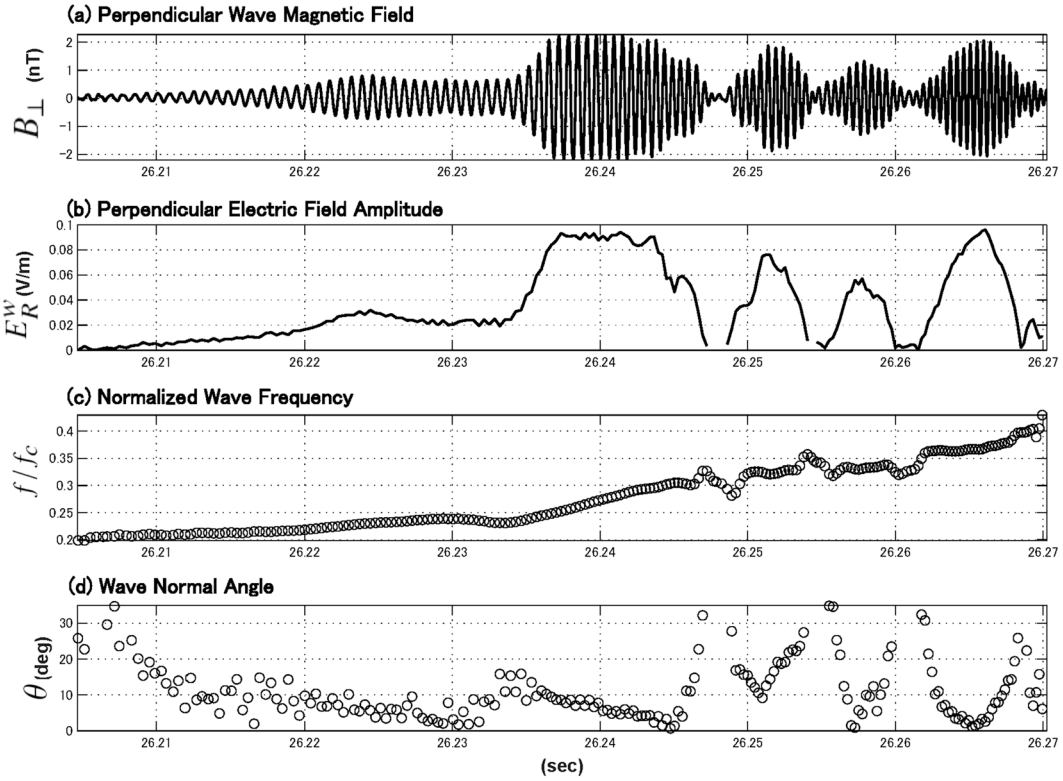

Figure 6. (a) Wave form of one of the perpendicular component of the magnetic field $B_\perp$ of the chorus element shown in Figure 5. (b) Electric field amplitude E_R^w of the R-mode wave component. (c) The normalized instantaneous frequency f/f_c obtained from the phase variation. (d) The wave normal angle θ obtained from the wave magnetic field.

7. Evaluation of Electron Acceleration Based on Wave Observations

We first calculate the interaction time ΔT_L for Landau resonant electrons to go through a half-wave cycle δt of the waveforms. The length of half the wavelength along the ambient magnetic field is given by $V_{g\|}\delta t$ where the parallel group velocity is given by (A22) of Hsieh and Omura (2017a). The interaction time is obtained by dividing half the wave length by the relative velocity between the wave packet moving with $V_{g\|}$ and a resonant electron moving with the parallel phase velocity $V_{p\|}$. We have

$$\Delta T_L = \frac{V_{g\|}\delta t}{|V_{g\|} - V_{p\|}|}\left(1 - \frac{V_{g\|}V_{p\|}}{c^2}\right), \tag{59}$$

where the relativistic effect for the relative velocity is included. Likewise, the interaction time ΔT_c for cyclotron resonant electrons is given by

$$\Delta T_c = \frac{V_{g\|}\delta t}{|V_{g\|} - V_R|}\left(1 - \frac{V_{g\|}V_R}{c^2}\right), \tag{60}$$

where $V_R = (\omega - \Omega/\gamma)/k_z$. Using (28) and the second-order resonance condition (35) for Landau resonance, we calculate the accelerations by the parallel E_z^w component and the perpendicular E_y^w component through Landau resonance as

$$\Delta K_{L\|} = -eE_z^w V_{p\|}\Delta T_L S_0 J_0(\beta_0), \tag{61}$$

and

$$\Delta K_{L\perp} = eE_y^w V_{\perp 0}\Delta T_L S_0 J_1(\beta_0), \tag{62}$$

respectively. The perpendicular velocity $V_{\perp 0}$ is calculated by

$$V_{\perp 0} = \sqrt{c^2(1-\gamma^{-2}) - V_{p\|}^2}, \tag{63}$$

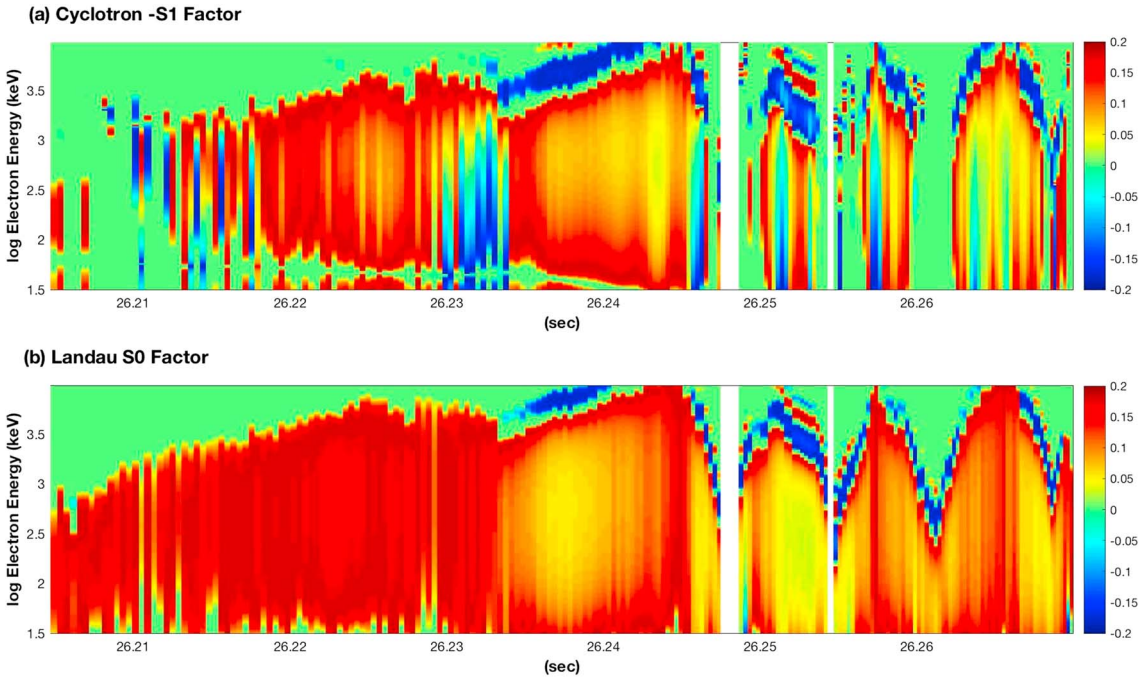

Figure 7. Inhomogeneity factors (a) S_1 and (b) S_0 at different energy and time for the chorus element shown in Figure 5.

and we can calculate

$$\beta_0 = \frac{\gamma V_{\perp 0} k_x}{\Omega_e}. \tag{64}$$

Similarly using (47) and the second-order resonance condition (55) for cyclotron resonance, we obtain accelerations by the parallel E_z^w component and the perpendicular components as

$$\Delta K_{c\parallel} = -eE_z^w V_R \Delta T_c S_1 J_1(\beta_1), \tag{65}$$

and

$$\Delta K_{c\perp} = -eV_{\perp 1} \Delta T_c S_1 [E_{\mathrm{R}}^w J_0(\beta_1) - E_{\mathrm{L}}^w J_2(\beta_1)], \tag{66}$$

respectively, where

$$V_{\perp 1} = \sqrt{c^2(1-\gamma^{-2}) - V_R^2}, \tag{67}$$

and

$$\beta_1 = \frac{\gamma V_{\perp 1} k_x}{\Omega_e}. \tag{68}$$

Using (9), we rewrite (66) as

$$\Delta K_{c\perp} = -e\frac{V_{\perp 1}}{2} \Delta T_c S_1 \{E_x^w [J_0(\beta_1) + J_2(\beta_1)] + E_y^w [J_0(\beta_1) - J_2(\beta_1)]\}. \tag{69}$$

In the cyclotron resonance, the acceleration by the perpendicular component $\Delta K_{c\perp}$ is much greater than that by the parallel component $\Delta K_{c\parallel}$, because $E_z^w << E_x^w, E_y^w$, $J_1(\beta_1) < J_0(\beta_1)$, and $V_R << V_{\perp 1}$ for quasi-parallel propagation, as we find in Figure 6 of Hsieh and Omura (2017a). In Landau resonance, the acceleration by the parallel component $\Delta K_{L\parallel}$ may play more significant contribution to the acceleration because $J_0(\beta_0)$, which is greater than $J_1(\beta_0)$ for $\beta_0 < 1$, is multiplied to the parallel component. For relativistic energies, however, we find $\Delta K_{L\parallel} << \Delta K_{L\perp}$ as is demonstrated with the data analysis of the observed chorus emission described below.

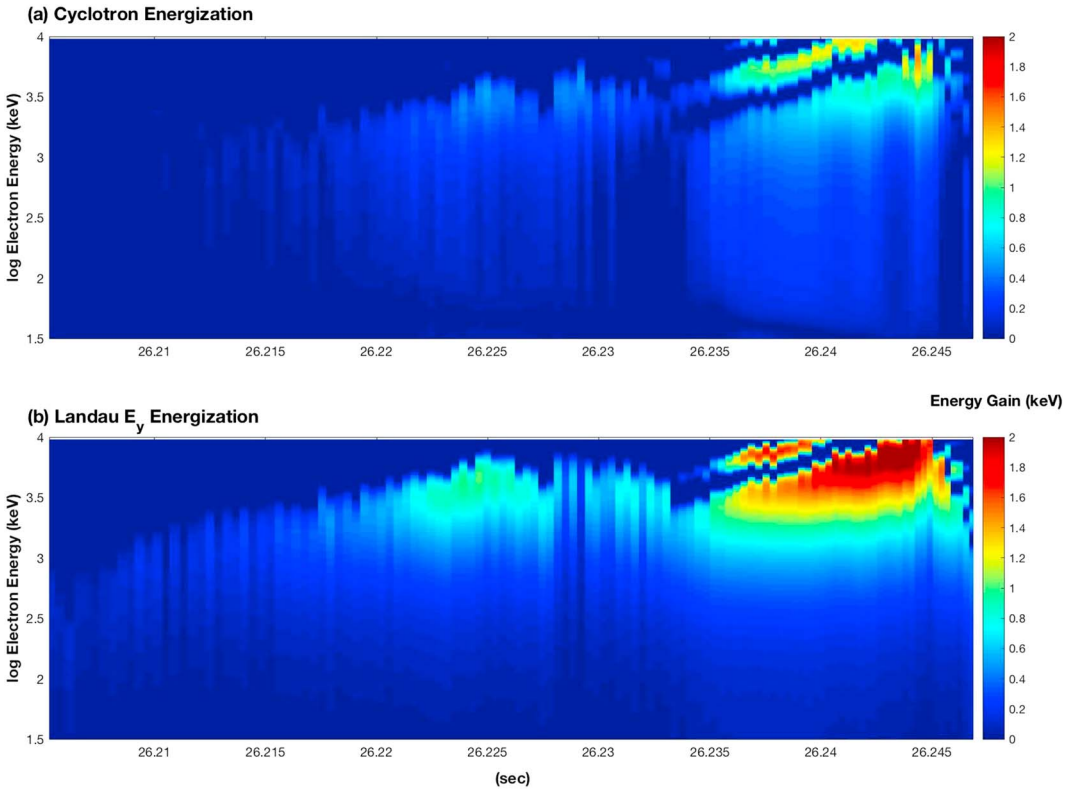

Figure 8. Energy gains over each half-wave period at different energy and times by (a) cyclotron resonance and (b) perpendicular electric field at Landau resonance.

The 17 March 2013 storm event was characterized by a deep (100×) dropout and rapid (1,000×) recovery of megaelectron volts outer zone radiation belt electron fluxes (Baker et al., 2014; Foster et al., 2014). Using the formulae derived above, we evaluate the efficiency of electron acceleration through interaction with chorus emissions observed with the Electric and Magnetic Field Instrument Suite and Integrated Science (Kletzing et al., 2013) onboard the twin Van Allen Probes satellites (also known as the Radiation Belt Storm Probes; Mauk et al., 2013). Figure 5 shows a strong rising-tone chorus observed by Van Allen Probe A at 16:56:26 UT on 17 March 2013. From the zero crossings of the perpendicular component of the wave magnetic field shown in Figure 6a, we can calculate instantaneous frequencies, which are plotted in Figure 6c. This is a lower-band chorus element with a range of frequency 0.2–0.32 f_c, where f_c is the local electron cyclotron frequency as shown in Figure 6c. The wave packet was generated near the magnetic equator and propagated away from the equator to the spacecraft location, undergoing convective wave growth especially at the higher frequency as shown in Figures 6a and 6b. The convective growth rates are higher for higher wave frequencies (Omura, Nakamura, et al., 2015).

With such a large amplitude coherent wave, we can expect nonlinear trapping of resonant electrons to take place. The necessary conditions for cyclotron and Landau resonant trappings are $|S_1| < 1$ and $|S_0| < 1$, respectively. Using (57) and (37), we calculated S_1 and S_0 for the chorus element discussed above and plotted them in Figures 7a and 7b, respectively. Both of them satisfy the condition for the nonlinear trappings with its maximum absolute values less than 0.2. The S_0 for Landau resonance mostly takes positive values because $\omega_{t1,0}^2$ given by (32) is negative.

The number of trapped particles decreases as $|S|$ increases from 0 to 1, because the size of the trapping potential shrinks to zero. The size of the trapping potential in the velocity phase space is given by

$$\frac{\Delta V}{V_{tr}} = \sqrt{\frac{\cos\zeta_1 - \cos\zeta_0 + (\zeta_0 - \zeta_1)S}{2}}, \tag{70}$$

where $\cos\zeta_0$ and $\cos\zeta_1$ are solutions of the second-order resonance conditions: $\sin\zeta + S = 0$, and V_{tr} is the trapping velocity, that is, the size of the potential around the resonance velocity for $S = 0$. The phases

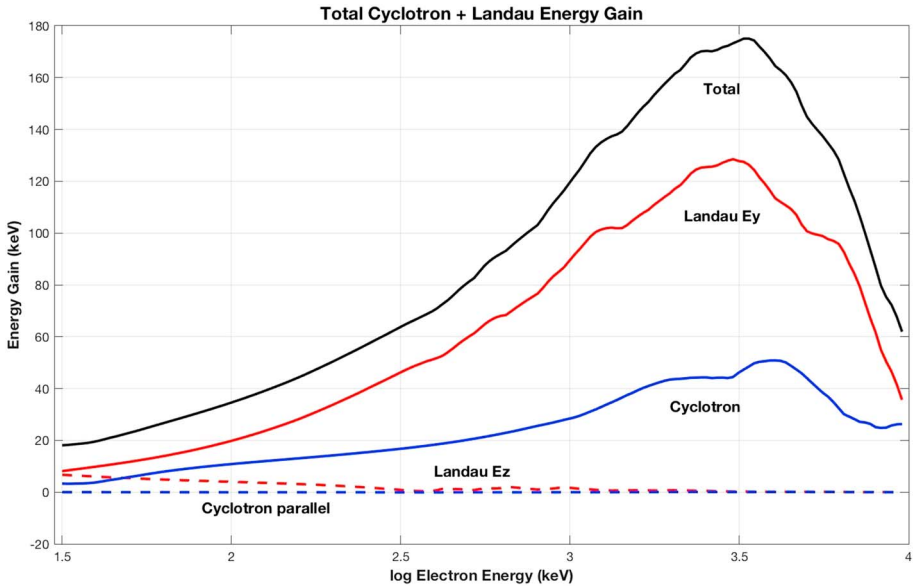

Figure 9. Energy gains through nonlinear trapping by the chorus element shown in Figure 5. Contributions by the parallel and perpendicular electric fields at Landau and cyclotron resonances and the total gain are plotted in different colors.

ζ_0 and ζ_1 are stable equilibrium point for trapped electrons and the saddle point for the separatrix of the trapping potential (Tobita & Omura, 2018). Since the trapping potential is two-dimensional in the velocity phase space, we can evaluate the number of trapped electrons by a function $F_t(S) = (\Delta V/V_{tr})^2$. Noting that $\zeta_0 = \pi + \arcsin S$ and $\zeta_1 = 2\pi - \arcsin S$ for $S > 0$, we obtain

$$F(S) = \sqrt{1 - S^2} + (\arcsin|S| - \frac{\pi}{2})|S|, \tag{71}$$

for $|S| < 1$, and we set $F(S) = 0$ for $|S| \geq 1$. We then multiply each of the accelerations (61), (62), (65), and (69) by $F(S)$ to evaluate corresponding energy gains. We have

$$G_{L\parallel} = \Delta K_{L\parallel} F(S_0), \quad G_{L\perp} = \Delta K_{L\perp} F(S_0), \tag{72}$$

for Landau resonance, and

$$G_{c\parallel} = \Delta K_{c\parallel} F(S_1), \quad G_{c\perp} = \Delta K_{c\perp} F(S_1), \tag{73}$$

for the cyclotron resonance.

The energy gains evaluated above are for each half-wave period δt. We plot $G_{c\perp}$ and $G_{L\perp}$ as functions of time with different electron kinetic energies in Figures 8a and 8b, respectively. The time period is for the duration of the chorus element shown in Figure 5.

By summing up each of the time series of energy gains throughout the chorus wave packet, we can estimate total energy gains through Landau and cyclotron resonances by the single chorus element as shown in Figure 9.

8. Summary and Discussion

We summarize results obtained by the present theoretical and observational studies on interaction between energetic electrons and whistler-mode chorus emissions as follows.

1. Efficient cyclotron acceleration of relativistic electrons takes place through Landau resonance with obliquely propagating whistler-mode chorus emissions. The perpendicular component E_y of the electric field plays major role in the Landau resonant cyclotron acceleration. It can be more efficient than that through cyclotron resonance because of the longer interaction time between the Landau resonant electron and the wave packet.

2. Formulae of Inhomogeneity factors S_0 and S_1 for Landau and cyclotron resonances have been derived theoretically, and they are tested with test particle simulations with a chorus element. Nonlinear trappings by Landau and cyclotron resonances are confirmed to take place when $0 < S_0 < 1$ and $-1 < S_1 < 0$, respectively.
3. In evaluating the efficiency of resonant electron acceleration in a chorus element observed by the Van Allen Probes, the values of S_0 and S_1 are calculated from the frequency sweep rates and the gradient of the local magnetic field. For substantial parts of the chorus element, we find $|S_0| < 1$ and $|S_1| < 1$, confirming the capability of nonlinear trapping by both Landau and cyclotron resonances.
4. In evaluating the total efficiency of electron acceleration by chorus, we have taken into account the probability of nonlinear trapping based on the sizes of the trapping potentials which are functions of the inhomogeneity factors.

We have demonstrated high efficiency of acceleration by chorus emissions with oblique wave normal angles, focusing on nonlinear trapping of resonant electrons through Landau and cyclotron resonances. The time scale of the electron acceleration is a duration period of a single chorus element as shown in Figure 5. Untrapped resonant electrons also contribute to the wave growth of chorus emissions giving energy to the waves, and some of them are scattered into the loss cone, resulting in microbursts. The generation process of chorus emissions has been studied by self-consistent simulations under an assumption of parallel propagation (Crabtree et al., 2017; Harid et al., 2014; Hikishima et al., 2009; Katoh & Omura, 2007, 2013; Nunn et al., 1997; Nunn & Omura, 2012; Tao, 2014). The overall efficiency of acceleration processes should be verified by self-consistent simulations in two-dimensional systems allowing propagation of oblique whistler-mode waves (Katoh, 2014; Ke et al., 2017).

As an effort to model the outer radiation belt, a long time evolution of the phase space density has been evaluated by the numerical Green's function method for parallel propagation (Kubota & Omura, 2018, Omura, Miyashita, et al., 2015), demonstrating rapid formation of the outer radiation belt. Some of the Green's functions for obliquely propagating chorus emissions have also been calculated (Hsieh & Omura, 2017a). More thorough construction of the Green's functions including oblique wave-particle interaction and simulations of long time evolution of the relativistic electron fluxes are left as future studies.

Acknowledgments
All wave data reported in this study can be obtained through the website (http://emfisis.physics.uiowa.edu). All simulation data are obtained from numerical integration of equations (7) and (9)–(11) in Hsieh and Omura (2017b). Computations were performed on the KDK system of the Research Institute for Sustainable Humanosphere (RISH) at Kyoto University. This work was supported by JSPS KAKENHI grants 15H05815 and 17H06140.

References

Artemyev, A. V., Agapitov, O., Mourenas, D., & Krasnoselskikh, V. V. (2016). Oblique whistler-mode waves in the Earth's inner magnetosphere: Energy distribution, origins, and role in radiation belt dynamics. *Space Science Reviews*, *200*, 261–355. https://doi.org/10.1007/s11214-016-02525

Artemyev, A. V., Vasiliev, A. A., Mourenas, D., Agapitov, O. V., & Krasnoselskikh, V. V. (2013). Nonlinear electron acceleration by oblique whistler waves: Landau resonance vs. cyclotron resonance. *Physics of Plasmas*, *20*, 122901. https://doi.org/10.1063/1.4836595

Baker, D. N., Jaynes, A. N., Li, X., Henderson, M. G., Kanekal, S. G., Reeves, G. D., et al. (2014). Gradual diffusion and punctuated phase space density enhancements of highly relativistic electrons: Van Allen Probes observations. *Geophysical Research Letters*, *41*, 1351–1358. https://doi.org/10.1002/2013GL058942

Bell, T. F., Inan, U. S., Haque, N., & Pickett, J. S. (2009). Source regions of banded chorus. *Geophysical Research Letters*, *36*, L11101. https://doi.org/10.1029/2009GL037629

Crabtree, C., Ganguli, G., & Tejero, E. (2017). Analysis of self-consistent nonlinear wave-particle interactions of whistler waves in laboratory and space plasmas. *Physics of Plasmas*, *24*, 056501. https://doi.org/10.1063/1.4977539

Foster, J. C., Erickson, P. J., Baker, D. N., Claudepierre, S. G., Kletzing, C. A., Kurth, W., et al. (2014). Prompt energization of relativistic and highly relativistic electrons during substorm intervals: Van Allen Probes observations. *Geophysical Research Letters*, *41*, 20–25. https://doi.org/10.1002/2013GL058438

Foster, J. C., Erickson, P. J., Omura, Y., Baker, D. N., Kletzing, C. A., & Claudepierre, S. G. (2017). Van Allen Probes Observations of prompt MeV radiation belt electron acceleration in non-linear interactions with VLF chorus. *Journal of Geophysical Research: Space Physics*, *121*, 324–339. https://doi.org/10.1002/2016JA023429

Ganguli, G., Rudakov, L., Crabtree, C., & Mithaiwala, M. (2012). Multi-pass whistler gain in a magnetospheric cavity due to induced nonlinear scattering. *Geophysical Research Letters*, *39*, L16105. https://doi.org/10.1029/2012GL052942

Habagishi, T., Yagitani, S., & Omura, Y. (2014). Nonlinear damping of chorus emissions at local half cyclotron frequencies observed by Geotail at L > 9. *Journal of Geophysical Research: Space Physics*, *119*, 4475–4483. https://doi.org/10.1002/2013JA019696

Harid, V., Golkowski, M., Bell, T., Li, J. D., & Inan, U. S. (2014). Finite difference modeling of coherent wave amplification in the Earth's radiation belts. *Geophysical Research Letters*, *41*, 8192–8200. https://doi.org/10.1002/2014GL061787

Hikishima, M., Yagitani, S., Omura, Y., & Nagano, I. (2009). Full particle simulation of whistler-mode rising chorus emissions in the magnetosphere. *Journal of Geophysical Research*, *114*, A01203. https://doi.org/10.1029/2008JA013625

Hsieh, Y.-K., & Omura, Y. (2017a). Nonlinear dynamics of electrons interacting with oblique whistler mode chorus in the magnetosphere. *Journal of Geophysical Research: Space Physics*, *122*, 675–694. https://doi.org/10.1002/2016JA023255

Hsieh, Y.-K., & Omura, Y. (2017b). Study of wave-particle interactions for whistler mode waves at oblique angles by utilizing the gyroaveraging method. *Radio Science*, *52*, 1268–128. https://doi.org/10.1002/2017RS006245

Hsieh, Y.-K., & Omura, Y. (2018). Nonlinear damping of oblique whistler mode waves via Landau resonance. *Journal of Geophysical Research: Space Physics*, *123*, 7462–7472. https://doi.org/10.1029/2018JA025848

Katoh, Y. (2014). A simulation study of the propagation of whistler-mode chorus in the Earth's inner magnetosphere. *Earth Planet Space*, *66*, 12. https://doi.org/10.1186/1880-5981-66-6

Katoh, Y., & Omura, Y. (2007). Computer simulation of chorus wave generation in the Earth's inner magnetosphere. *Geophysical Research Letters*, *34*, L03102. https://doi.org/10.1029/2006GL028594

Katoh, Y., & Omura, Y. (2013). Effect of the background magnetic field inhomogeneity on generation processes of whistler-mode chorus and broadband hiss-like emissions. *Journal of Geophysical Research: Space Physics*, *118*, 4189–4198. https://doi.org/10.1002/jgra.50395

Ke, Y., Gao, X., Lu, Q., Wang, X., & Wang, S. (2017). Generation of risingtone chorus in a two-dimensional mirror field by using the general curvilinear PIC code. *Journal of Geophysical Research: Space Physics*, *122*, 675–694. https://doi.org/10.1002/2017JA024178

Kletzing, C. A., Kurth, W. S., Acuna, M., MacDowall, R. J., Torbert, R. B., Averkamp, T., et al. (2013). The Electric and Magnetic Field Instrument Suite and Integrated Science (EMFISIS) on RBSP. *Space Science Reviews*, *179*, 127–181. https://doi.org/10.1007/s11214-013-9993-6

Kubota, Y., & Omura, Y. (2018). Nonlinear dynamics of radiation belt electrons interacting with chorus emissions localized in longitude. *Journal of Geophysical Research: Space Physics*, *123*, 4835–4857. https://doi.org/10.1029/2017JA025050

Kurita, S., Katoh, Y., Omura, Y., Angelopoulos, V., Cully, C. M., Le Contel, O., & Misawa, H. (2012). THEMIS observation of chorus elements without a gap at half the gyrofrequency. *Journal of Geophysical Research*, *117*, A11223. https://doi.org/10.1029/2012JA018076

Li, W., Bortnik, J., Thorne, R. M., & Angelopoulos, V. (2011). Global distribution of wave amplitudes and wave normal angles of chorus waves using THEMIS wave observations. *Journal of Geophysical Research*, *116*, A12205. https://doi.org/10.1029/2011JA017035

Li, W., Santolik, O., Bortnik, J., Thorne, R. M., Kletzing, C. A., Kurth, W. S., & Hospodarsky, G. B. (2016). New chorus wave properties near the equator from Van Allen Probes wave observations. *Geophysical Research Letters*, *43*, 4725–4735. https://doi.org/10.1002/2016GL068780

Li, W., Thorne, R. M., Angelopoulos, V., Bortnik, J., Cully, C. M., Ni, B., et al. (2009). Global distribution of whistler-mode chorus waves observed on the THEMIS spacecraft. *Geophysical Research Letters*, *36*, L09104. https://doi.org/10.1029/2009GL037595

Mauk, B. H., Fox, N. J., Kanekal, S. G., Kessel, R. L., Sibeck, D. G., & Ukhorskiy, A. (2013). Science objectives and rationale for the Radiation Belt Storm Probes mission. *Space Science Reviews*, *179*(1–4), 3–27. https://doi.org/10.1007/s11214-012-9908-y

Nunn, D., & Omura, Y. (2012). A computational and theoretical analysis of falling frequency VLF emissions. *Journal of Geophysical Research*, *117*, A08228. https://doi.org/10.1029/2012JA017557

Nunn, D., & Omura, Y. (2015). A computational and theoretical investigation of nonlinear wave-particle interactions in oblique whistlers. *Journal of Geophysical Research: Space Physics*, *120*, 2890–2911. https://doi.org/10.1002/2014JA020898

Nunn, D., Omura, Y., Matsumoto, H., Nagano, I., & Yagitani, S. (1997). The numerical simulation of VLF chorus and discrete emissions observed on the Geotail Satellite using a Vlasov code. *Journal of Geophysical Research*, *102*, 27,083–27,097.

Omura, Y., Furuya, N., & Summers, D. (2007). Relativistic turning acceleration of resonant electrons by coherent whistler mode waves in a dipole magnetic field. *Journal of Geophysical Research*, *112*, A06236. https://doi.org/10.1029/2006JA012243

Omura, Y., Hikishima, M., Katoh, Y., Summers, D., & Yagitani, S. (2009). Nonlinear mechanisms of lower-band and upper-band VLF chorus emissions in the magnetosphere. *Journal of Geophysical Research*, *114*, A07217. https://doi.org/10.1029/2009JA014206

Omura, Y., Katoh, Y., & Summers, D. (2008). Theory and simulation of the generation of whistler-mode chorus. *Journal of Geophysical Research*, *113*, A04223. https://doi.org/10.1029/2007JA012622

Omura, Y., Miyashita, Y., Yoshikawa, M., Summers, D., Hikishima, M., Ebihara, Y., & Kubota, Y. (2015). Formation process of relativistic electron flux through interaction with chorus emissions in the Earth's inner magnetosphere. *Journal of Geophysical Research: Space Physics*, *120*, 9545–9562. https://doi.org/10.1002/2015JA021563

Omura, Y., Nakamura, S., Kletzing, C. A., Summers, D., & Hikishima, M. (2015). Nonlinear wave growth theory of coherent hiss emissions in the plasmasphere. *Journal of Geophysical Research: Space Physics*, *120*, 7642–7657. https://doi.org/10.1002/2015JA021520

Omura, Y., & Nunn, D. (2011). Triggering process of whistler mode chorus emissions in the magnetosphere. *Journal of Geophysical Research*, *116*, A05205. https://doi.org/10.1029/2010JA016280

Omura, Y., Nunn, D., & Summers, D. (2012). Generation processes of whistler-mode chorus emissions: Current status of nonlinear wave growth theory. In D. Summers (Ed.), *Dynamics of the Earth's radiation belts and inner magnetosphere, Geophysical Monograph Series* (Vol. 199). Washington, DC: American Geophysical Union. https://doi.org/10.1029/2012GM001347

Omura, Y., & Zhao, Q. (2012). Nonlinear pitch angle scattering of relativistic electrons by EMIC waves in the inner magnetosphere. *Journal of Geophysical Research*, *117*, A08227. https://doi.org/10.1029/2012JA017943

Shklyar, D., & Matsumoto, H. (2009). Oblique whistler-mode waves in the inhomogeneous magnetospheric plasma: Resonant interactions with energetic charged particles. *Surveys in Geophysics*, *30*, 55–104. https://doi.org/10.1007/s10712-009-9061-7

Shoji, M., & Omura, Y. (2013). Triggering process of electromagnetic ion cyclotron rising tone emissions in the inner magnetosphere. *Journal of Geophysical Research: Space Physics*, *118*, 5553–5561. https://doi.org/10.1002/jgra.50523

Stix, T. H. (1992). *Waves in plasmas*. New York: Am. Inst. of Phys.

Summers, D., & Omura, Y. (2007). Ultra-relativistic acceleration of electrons in planetary magnetospheres. *Geophysical Research Letters*, *34*, L24205. https://doi.org/10.1029/2007GL032226

Tao, X. (2014). A numerical study of chorus generation and the related variation of wave intensity using the DAWN code. *Journal of Geophysical Research: Space Physics*, *119*, 3362–3372. https://doi.org/10.1002/2014JA019820

Tobita, M., & Omura, Y. (2018). Nonlinear dynamics of resonant electrons interacting with coherent Langmuir waves. *Physics of Plasmas*, *25*, 032105. https://doi.org/10.1063/1.5018084

Yagitani, S., Habagishi, T., & Omura, Y. (2014). Geotail observation of upper band and lower band chorus elements in the outer magnetosphere. *Journal of Geophysical Research: Space Physics*, *119*, 4694–4705. https://doi.org/10.1002/2013JA019678